

A UNIFIED GAS-KINETIC PARTICLE METHOD FOR MULTISCALE PHOTON TRANSPORT*

WEIMING LI[†], CHANG LIU[‡], YAJUN ZHU[§], JIWEI ZHANG[¶], AND KUN XU^{||}

Abstract. In this work, we present a unified gas-kinetic particle (UGKP) method for the simulation of multiscale photon transport. The multiscale nature of the particle method mainly comes from the recovery of the time evolution flux function in the unified gas-kinetic scheme (UGKS) through a coupled dynamic process of particle transport and collision. This practice improves the original operator splitting approach in the Monte Carlo method, such as the separated treatment of particle transport and collision. As a result, with the variation of the ratio between numerical time step and local photon's collision time, different transport physics can be fully captured in a single computation. In the diffusive limit, the UGKP method could recover the solution of the diffusion equation with the cell size and time step being much larger than the photon's mean free path and the mean collision time. In the free transport limit, it presents an exact particle tracking process as the original Monte Carlo method. In the transition regime, the weights of particle free transport and collision are determined by the ratio of local numerical time step to the photon's collision time. Several one-dimensional numerical examples covering all transport regimes from the optically thin to optically thick are computed to validate the accuracy and efficiency of the current scheme. In comparison with the S_N discrete ordinate method, the UGKP method is based on particles and avoids the discretization of particle velocity space, which does not suffer from the ray effect.

Key word. radiative transfer equations, diffusion equation, asymptotic preserving, Monte Carlo particle method, unified gas-kinetic scheme

1. Introduction. The radiative transfer equation describes photon propagation in the background medium and has important applications in the fields of astrophysics [5], atmospheric physics [23], optical imaging [19] and so on. In this paper, we focus on the gray radiative transfer equation with isotropic scattering, which reads

$$(1.1) \quad \frac{1}{c} \frac{\partial I}{\partial t} + \boldsymbol{\Omega} \cdot \nabla I = \sigma_s \left(\frac{1}{4\pi} \int_{\mathbb{S}^2} I d\boldsymbol{\Omega} - I \right) - \sigma_a I + G,$$

where $I(t, \mathbf{x}, \boldsymbol{\Omega})$ is the specific intensity which depends on time t , space $\mathbf{x} \in \mathbb{R}^3$, and angle $\boldsymbol{\Omega}$, while c is the speed of light, σ_s is the scattering coefficient, σ_a is the absorption coefficient, and G is an internal source of photons.

There are typically two categories of numerical methods for solving the radiative transfer equations. The first category consists of the deterministic methods with different ways of discretizing and modeling, such as the discrete ordinate method [14, 4, 3, 26] and the moment methods [11, 2, 32, 1]. The second category consists of the stochastic approach, for example, the Monte Carlo method [10, 22, 13]. The Monte Carlo method is a very popular method for solving the radiative transfer problems. In comparison with the deterministic methods,

*Submitted to the editors October 14, 2018.

Funding: The current research is supported by Hong Kong research grant council (16207715, 16206617), National Science Foundation of China (11772281, 91530319, 11771035), and NSAF U1530401.

[†]Applied and Computational Mathematics Division, Beijing Computational Science Research Center, Beijing 100193, China and Department of Mathematics, Hong Kong University of Science and Technology, Clear Water Bay, Kowloon, Hong Kong, China. (liweiming@csrc.ac.cn).

[‡]Department of Mathematics, Hong Kong University of Science and Technology, Clear Water Bay, Kowloon, Hong Kong, China. (cliuaa@connect.ust.hk).

[§]National Key Laboratory of Science and Technology on Aerodynamic Design and Research, Northwestern Polytechnical University, Xi'an, Shaanxi 710072, China. (zhuyajun@mail.nwpu.edu.cn).

[¶]Applied and Computational Mathematics Division, Beijing Computational Science Research Center, Beijing 100193, China. (jwzhang@csrc.ac.cn).

^{||}Corresponding author. Department of Mathematics, Hong Kong University of Science and Technology, Clear Water Bay, Kowloon, Hong Kong, China and Department of Mechanical and Aerospace Engineering, Hong Kong University of Science and Technology, Clear Water Bay, Kowloon, Hong Kong, China. (makxu@ust.hk).

it is more efficient in optically thin regime especially for the multidimensional cases, and it does not suffer from the ray effect. However, it has difficulties when it comes to diffusive regime. In diffusive regime where the mean free path is small, photons may go through a huge number of scatterings during their lifetimes. Direct simulation of each scattering process for all particles makes the Monte Carlo method very expensive in the diffusive regime.

On the other hand, in the diffusive regime the photon transport process could be well described by the diffusion equation, which could be solved efficiently. Based on this observation, many hybrid methods have been developed in order to improve the overall efficiency in different regimes [9, 12, 8, 7], where the Monte Carlo method is used in the optically thin regions and the diffusion equation is applied to the optically thick regions. However, as far as we know, there is still no unifying principle for accurate domain decomposition for different regimes.

Another approach towards releasing the stiffness issue in the diffusive regime is to develop asymptotic-preserving (AP) schemes [18, 25, 15, 17, 24, 27, 31, 29, 28, 30]. One of the examples is the unified gas-kinetic scheme (UGKS), which couples the particles' transport and collision process using a multiscale flux function obtained from the integral solution of the kinetic model equation. The cell size and time step are not restricted by the mean free path and mean collision time. It was developed initially in the field of rarefied gas dynamics [34, 33] and has been applied to the field of radiative transfer [24, 27, 31, 29, 28, 30], plasma transport [21] and disperse multi-phase flow [20]. Since it is a discrete ordinate based numerical scheme, it has no statistical noise, but unavoidably suffers from the ray effect.

In this work, we combine the advantages of the UGKS and the Monte Carlo method, and develop a novel unified gas-kinetic particle (UGKP) method to describe the multiscale photon transport. In our method, the photons are described by the particle transport and collision, and this process is controlled by a multiscale transport solution in all regimes. More specifically, the Monte Carlo particle model is used to discretize the angular direction of the photon's movement. Based on the particles' transport nature in the discretize physical space, particles are categorized into three groups. Given a fixed time step, the freely transported particles are accurately tracked by following the trajectories of the simulation particles, while those particles that suffer collision within the given time step are grouped and re-sampled according to the macroscopic variables at the new time level. The fluxes across a cell interface from different type particles are taken into account for the updating of cell averaged macroscopic variables. In such a way, the multiscale process through particles' transport and their interaction through macroscopic hydrodynamics is recovered. The multiscale flux function of the UGKS is precisely preserved in the particle implementation. In the diffusive regime, the resulting algorithm would become a standard central difference scheme for the diffusion equation. In the optically thin regime, it gives a particle tracking method same as the Monte Carlo method. In the transition regime, the ratio of the time step over particle collision time determines the transport dynamics between the above two limits.

The rest of this paper is organized as follows. Section 2 briefly recalls the basic idea of the unified gas-kinetic scheme (UGKS) for the linear transport equation. Section 3 presents the UGKP method for linear photon transport and the gray radiative transfer equations. In Section 4, numerical tests are presented to demonstrate the accuracy and robustness of the particle method. The final section is the conclusion.

2. Review of the UGKS for the linear transport equation. The unified gas-kinetic scheme (UGKS) was initially developed for the problems in the field of rarefied gas dynamics [34, 33], and have also been successfully applied to problems in radiative transfer under the finite volume framework [24, 27, 31, 29, 28, 30]. In this section, we review the basic idea of the UGKS using the example of the one-dimensional linear transport equation in a purely

scattering medium.

Consider

$$(2.1) \quad \frac{1}{c} \frac{\partial I}{\partial t} + \mu \frac{\partial I}{\partial x} = \sigma \left(\frac{1}{2} \int_{-1}^1 I \, d\mu - I \right),$$

which give a non-dimensional equation

$$(2.2) \quad \epsilon \frac{\partial I}{\partial t} + \mu \frac{\partial I}{\partial x} = \frac{\sigma}{\epsilon} \left(\frac{1}{2} E - I \right),$$

where $E = \int_{-1}^1 I(\mu) \, d\mu$. We employed the same non-dimensionalization process as [24].

The UGKS is based on a finite volume framework. We assume uniform mesh for simplicity of discussion. Define

$$(2.3) \quad I_j^n = \frac{1}{\Delta x} \int_{x_{j-\frac{1}{2}}}^{x_{j+\frac{1}{2}}} I(t_n, x, \mu) \, dx$$

to be the averaged specific intensity I over a spatial cell, and

$$(2.4) \quad E_j^n = \frac{1}{\Delta x} \int_{x_{j-\frac{1}{2}}}^{x_{j+\frac{1}{2}}} E(t_n, x) \, dx$$

to be the averaged energy density function E over a spatial cell. Under the finite volume framework, the discretizations of the microscopic and macroscopic governing equations give

$$(2.5) \quad \frac{I_j^{n+1} - I_j^n}{\Delta t} + \frac{1}{\Delta x} (\phi_{j+\frac{1}{2}} - \phi_{j-\frac{1}{2}}) = \frac{\sigma}{\epsilon^2} (E_j^{n+1} - I_j^{n+1}),$$

and

$$(2.6) \quad \frac{E_j^{n+1} - E_j^n}{\Delta t} + \frac{1}{\Delta x} (\Phi_{j+\frac{1}{2}} - \Phi_{j-\frac{1}{2}}) = 0,$$

where the microscopic and macroscopic flux terms are respectively

$$(2.7) \quad \phi_{j+\frac{1}{2}} = \frac{1}{\epsilon \Delta t} \int_{t_n}^{t_{n+1}} \mu I(t, x_{j+\frac{1}{2}}, \mu) \, dt,$$

and

$$(2.8) \quad \Phi_{j+\frac{1}{2}} = \int_{-1}^1 \phi_{j+\frac{1}{2}}(\mu) \, d\mu.$$

The key ingredient of the UGKS is the construction of the multiscale flux function by adopting the integral solution of the kinetic model equation (2.2). Assuming a local constant σ , the integral solution of equation (2.2) along the characteristic line gives

$$(2.9) \quad \begin{aligned} I(t, x_{j+\frac{1}{2}}, \mu) = & e^{-\frac{\sigma_{j+\frac{1}{2}}(t-t_n)}{\epsilon^2}} I\left(t_n, x_{j+\frac{1}{2}} - \frac{\mu}{\epsilon}(t-t_n)\right) \\ & + \int_{t_n}^t e^{-\frac{\sigma_{j+\frac{1}{2}}(t-s)}{\epsilon^2}} \times \frac{\sigma_{j+\frac{1}{2}}}{\epsilon^2} \frac{1}{2} E\left(s, x_{j+\frac{1}{2}} - \frac{\mu}{\epsilon}(t-s)\right) \, ds, \end{aligned}$$

which is used to construct the numerical fluxes in equation (2.5). The integral solution couples transport with particle collisions, and bridges the kinetic and the hydrodynamic scale dynamics.

The numerical fluxes for microscopic and macroscopic variable updates are based on the piecewise linear initial reconstruction of I and E at the beginning of each time step. The details were presented in [24] and [27]. It has been proved in [24] that when σ equals 0, the UGKS tends to the finite volume scheme

$$(2.10) \quad \frac{I_j^{n+1} - I_j^n}{\Delta t} + \frac{1}{\Delta x} \frac{\mu}{\epsilon} \left((I_j^n 1_{\mu>0} + I_{j+1}^n 1_{\mu<0}) - (I_{j-1}^n 1_{\mu>0} + I_j^n 1_{\mu<0}) \right) = 0,$$

which is consistent with free transport solution. In the diffusion limit, with a uniform mesh the UGKS scheme becomes

$$(2.11) \quad \frac{E_j^{n+1} - E_j^n}{\Delta t} - \frac{1}{\Delta x} \left(\frac{1}{3\sigma_{j+\frac{1}{2}}} \frac{E_{j+1}^{n+1} - E_j^{n+1}}{\Delta x} - \frac{1}{3\sigma_{j-\frac{1}{2}}} \frac{E_j^{n+1} - E_{j-1}^{n+1}}{\Delta x} \right) = 0,$$

which is a standard central difference scheme for the limit diffusion equation as ϵ tends to 0. For more details on the asymptotic analysis of the UGKS for the radiative transfer equation we refer to [24] and [27].

Following the methodology of the UGKS, we will construct a particle algorithm with multiscale transport property for recovering transport physics from the kinetic scale to the hydrodynamic scale. For the kinetic scale particle free transport, the method tracks the particle trajectory precisely; for those particles suffering collisions, the updated macroscopic variables will be used to re-sample them. A multiscale particle method for equations (2.8), (2.7), and (2.9) is constructed through the tracking and re-sampling particles with the help of updated macroscopic variables.

3. Multiscale Particle Method. In this section, we will first show the physical picture for the particle classification and evolution. Then, the multiscale particle algorithm will be introduced. This algorithm is first presented for a single linear transport equation; then it will be extended to the standard one-group radiative transfer and material temperature equations.

3.1. Classification of particles. The particles can move freely until they interact with background medium. Based on the process of transport and collision, the particles can be divided into three types, which are denoted as Type I, Type II, and Type III particles. Type I particles travel freely within the entire time step. Type II particles travel freely across a cell interface before they collide with the background medium. Type III particles collide with the background medium before they reach the cell interface. Note that within a whole time step any particle of the three types can stay in the same cell or move to the neighboring cell. More specifically, Type I particles may transport freely to the neighboring cell during the time step, or they transport to another place within the same cell. Type II particles may move freely to the neighboring cell, collide with the background medium, and then remain in the same cell for the rest of the time step, or they may bounce back to their former cell or transport to another neighboring cell after collision. Type III particles may stay in the same cell after their first collision with the background medium until the end of the time step, or they may move across the cell interface before the end of the time step. This classification of particles is illustrated in Figure 3.1, where Type I particles are denoted by white circles, Type II particles by grey circles, and Type III particles by black circles. Denoting t_c as the time for the first collision event for each particle and t_{in} as the time for each particle to freely transport until it reaches the cell interface, the conditions for classification of particles are summarized in Table 3.1.

Note that the UGKS solves the linear kinetic equation by a finite volume method and the flux terms are approximated by Eq.(2.9). In order to recover the multiscale transport in Eq.(2.9), the free transport process of Type I and Type II particles mimics the first term in

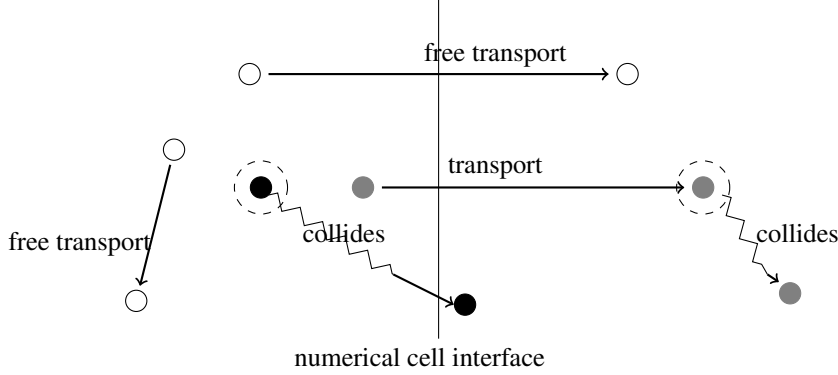


FIG. 3.1. Diagram for classification of particles.

TABLE 3.1
Classification of particles.

Particle type	Condition
Type I	$t_c > \Delta t$
Type II	$\Delta t > t_c > t_{in}$
Type III	$t_c < \Delta t$ & $t_c < t_{in}$

Eq.(2.9), while the collision effect of Type II and Type III particles simulate the second term in (2.9). In this way, we can recover the UGKS flux through particle implementation. Type I particles and the free transport process of Type II particles can be tracked precisely, while Type II particles after collision and Type III particles are grouped and are re-sampled from macroscopic variables due to their close connection to the equilibrium state. The detailed implementation is given in Section 3.2.

3.2. The unified gas-kinetic particle method. Under the Monte Carlo framework, the specific intensity $I(t, x, \mu)$ is represented by a finite number of simulation particles. For each particle, the unknown variables are its position, velocity, and weight, denoted as the 3-tuple (x_j, μ_j, w_j) . The computation domain is divided into cells to locate particles and sample the local macroscopic quantities. Denote E_m as the average of the macroscopic energy density within cell m , V_m as the volume of cell m , and w_j as the weight of the j -th particle within the same cell. Denote N_m as the number of simulation particles within cell m . Then, the macroscopic quantities and the corresponding particle information satisfy the following relationship:

$$(3.1) \quad E_m = \frac{1}{V_m} \sum_{j=1}^{N_m} w_j.$$

This section considers the particle method for solving equation (2.2), which is the linear equation with purely scattering medium. The extension of the method to the radiation-material coupled equations will be discussed in Section 3.4.

With the approximation of σ as a local constant value σ_j and using an implicit approximation to E , Eq. (2.9) can be modeled as

$$(3.2) \quad I(t_{n+1}, x) = e^{-\frac{\sigma}{c^2} \Delta t} I\left(t_n, x - \frac{\mu}{c} \Delta t\right) + (1 - e^{-\frac{\sigma}{c^2} \Delta t}) \frac{1}{2} E(t_{n+1}, x).$$

Eq. (3.2) could be implemented under the particle Monte Carlo framework. For a fixed time step Δt , each particle is allowed to transport freely under probability $e^{-\frac{\sigma}{\epsilon^2}\Delta t}$. At the same time, with the probability $1 - e^{-\frac{\sigma}{\epsilon^2}\Delta t}$, the particle is re-sampled from the equilibrium distribution at the new time step. The algorithm consists of the following steps: the free transportation of particle is precisely followed and contributes to the kinetic scale fluxes. Together with the hydrodynamic scale fluxes obtained from the equilibrium state, the macroscopic variables can be updated first, then the updated macroscopic quantities guide the updating of the microscopic particle distribution. In the above procedures, both macroscopic and microscopic quantities will be updated within each control volume. In the next section, the details for updating macroscopic variable will be discussed.

3.2.1. Updating macroscopic quantity. To simplify discussions, the method will be given under the assumption of the uniform mesh. Its extension to non-uniform mesh is straightforward. Eq. (2.6) for updating the macroscopic variable can be re-written as

$$(3.3) \quad E_j^{n+1} = E_j^n - \frac{\Delta t}{\Delta x} (\Phi_{j+\frac{1}{2}} - \Phi_{j-\frac{1}{2}}).$$

The interface fluxes (2.8) are based on the solution of Eq. (2.9),

$$(3.4) \quad \begin{aligned} \Phi_{j+\frac{1}{2}} = & \frac{1}{\epsilon\Delta t} \int_{t_n}^{t_{n+1}} \int_{-1}^1 \mu e^{-\frac{\sigma_{j+\frac{1}{2}}(t-t_n)}{\epsilon^2}} I\left(t_n, x_{j+\frac{1}{2}} - \frac{\mu}{\epsilon}(t-t_n), \mu\right) d\mu dt \\ & + \frac{1}{2\epsilon\Delta t} \int_{t_n}^{t_{n+1}} \int_{t_n}^t \int_{-1}^1 \mu \frac{\sigma_{j+\frac{1}{2}}}{\epsilon^2} e^{-\frac{\sigma_{j+\frac{1}{2}}(t-s)}{\epsilon^2}} E\left(s, x_{j+\frac{1}{2}} - \frac{\mu}{\epsilon}(t-s)\right) ds d\mu dt. \end{aligned}$$

With the piecewise linear reconstruction for E ,

$$(3.5) \quad \begin{aligned} E\left(s, x_{j+\frac{1}{2}} - \frac{\mu}{\epsilon}(t-s)\right) = & E(t_{n+1}, x_{j+\frac{1}{2}}) + \frac{\partial E}{\partial t}(t_{n+1}, x_{j+\frac{1}{2}}) \times (s - t_{n+1}) \\ & + \frac{\partial E}{\partial x}(t_{n+1}, x_{j+\frac{1}{2}}) \times \left(-\frac{\mu}{\epsilon}(t-s)\right), \end{aligned}$$

the implicit central difference discretization for $\frac{\partial E}{\partial x}$,

$$(3.6) \quad \frac{\partial E}{\partial x}(t_{n+1}, x_{j+\frac{1}{2}}) \approx \frac{E_{j+1}^{n+1} - E_j^{n+1}}{\Delta x},$$

and the direct computation

$$(3.7) \quad \begin{aligned} & \int_{t_n}^{t_{n+1}} \left(\int_{t_n}^t (t-s) e^{-\frac{\sigma(t-s)}{\epsilon^2}} ds \right) dt \\ & = \frac{1}{\left(\frac{\sigma}{\epsilon^2}\right)^2} \left(-\frac{2}{\left(\frac{\sigma}{\epsilon^2}\right)} \left(1 - e^{-\frac{\sigma\Delta t}{\epsilon^2}}\right) + \Delta t \left(1 + e^{-\frac{\sigma\Delta t}{\epsilon^2}}\right) \right), \end{aligned}$$

the update E^{n+1} in Eq. (3.3) becomes

$$(3.8) \quad \frac{\Delta t}{\Delta x^2} \alpha_{j-\frac{1}{2}} E_{j-1}^{n+1} + \left(1 - \frac{\Delta t}{\Delta x^2} (\alpha_{j-\frac{1}{2}} + \alpha_{j+\frac{1}{2}})\right) E_j^{n+1} + \frac{\Delta t}{\Delta x^2} \alpha_{j+\frac{1}{2}} E_{j+1}^{n+1} = r.h.s,$$

where

$$(3.9) \quad \alpha_{j+\frac{1}{2}} = -\frac{1}{3\sigma_{j+\frac{1}{2}}} \left(-\frac{2}{\left(\frac{\sigma_{j+\frac{1}{2}}\Delta t}{\epsilon^2}\right)} \left(1 - e^{-\frac{\sigma_{j+\frac{1}{2}}\Delta t}{\epsilon^2}}\right) + \left(1 + e^{-\frac{\sigma_{j+\frac{1}{2}}\Delta t}{\epsilon^2}}\right) \right),$$

and

$$(3.10) \quad \begin{aligned} r.h.s = E_j^n &+ \frac{1}{\Delta x} \int_{-1}^1 \int_{t_n}^{t_{n+1}} \frac{\mu}{\epsilon} e^{-\frac{\sigma_{j-\frac{1}{2}}(t-t_n)}{\epsilon^2}} I\left(t_n, x_{j-\frac{1}{2}} - \frac{\mu}{\epsilon}(t-t_n), \mu\right) dt d\mu \\ &- \frac{1}{\Delta x} \int_{-1}^1 \int_{t_n}^{t_{n+1}} \frac{\mu}{\epsilon} e^{-\frac{\sigma_{j+\frac{1}{2}}(t-t_n)}{\epsilon^2}} I\left(t_n, x_{j+\frac{1}{2}} - \frac{\mu}{\epsilon}(t-t_n), \mu\right) dt d\mu. \end{aligned}$$

The Monte Carlo implementation of the right hand side of Eq. (3.10) for the computation of the fluxes is about calculating the freely transported particles across the cell interface, and the number of particles across the interface is computed during the transport process while taking into account the possible particle collisions. After determining its right hand side, Eq. (3.8) can be solved to get E^{n+1} . Subsequently, it can be used to re-sample particles.

3.2.2. Updating particle distribution. For updating particle distribution, the free transport process of Type I and Type II particles before collision with background medium are tracked precisely. The influence of the collision process on the particle distribution (Type II and Type III particles) is considered by re-sampling according to the equilibrium distribution at the new time step. We denote W to be the total energy density of Type II and Type III particles. Our algorithm for updating particle information within each time step is as follows:

1. At the beginning of a time step, set the macroscopic variable W to zero.
2. Perform the following for all particles: for each particle, generate time t_c at which the first collision event happens according to the local σ . There are three possible scenarios:
 - (a) If $t_c > \Delta t$, the particle is allowed to transport freely.
 - (b) If $\Delta t > t_c > t_{in}$, the weight of the particle is added to W of the neighbouring cell where the particle goes.
 - (c) If $t_c < t_{in}$ and $t_c < \Delta t$, the weight of the particle is added to W of the current cell.
3. Add the contribution to W in the cells through the macroscopic flux $\Phi_{j+\frac{1}{2}}$ denoted as Φ_E ,

$$(3.11) \quad \Phi_{E,j+\frac{1}{2}} = \alpha_{j+\frac{1}{2}} \frac{E_{j+1}^{n+1} - E_j^{n+1}}{\Delta x}.$$

4. Generate particles according to the equilibrium distribution constructed from W . Specifically, a piecewise linear reconstruction of W is constructed first. Then, the position of the particles are sampled according to the distribution of W in space, while the microscopic velocities of the particles are sampled according to a uniform distribution on $[-1, 1]$.

REMARK 3.1. *Due to the stochastic noise and high order reconstruction of W , when W is very close to zero, its numerical values could sometimes be negative. This could be treated either by setting W to zero, or by generating particles with negative weights.*

3.2.3. Outline of the algorithm. In this section, we give a brief summary of the implementation of the unified gas-kinetic particle method.

Upon initialization, we use a weight factor w_p to indicate the amount of photon energy represented by each simulation particle. Given the initial condition of E in cell m , one can obtain the number of particles N_m by

$$(3.12) \quad N_m = \frac{E_m V_m}{w_p}.$$

Then, the local initial distribution function $I(t_0, x_j, \mu)$ is applied to generate N_m particles and their initial velocities. Given the information of particles and the macroscopic energy

density, the system would then be evolved to the next time step by Algorithm 3.1. This is done for each time step until the end of computation.

Algorithm 3.1 The unified gas-kinetic particle method within one time step Δt .

Input:

- The set of (x_i, μ_i, w_i) for all particles at time $t = t_n$;
- The set of macroscopic variables E_j for all spatial cells at time $t = t_n$;

Output:

- The set of (x_i, μ_i, w_i) for all particles at time $t = t_{n+1}$;
 - The set of macroscopic variables E_j for all spatial cells at time $t = t_{n+1}$;
 - 1: Set the macroscopic variable for re-sampling. W is 0 for all spatial cells and N_{total} is the total current number of simulation particles;
 - 2: **for** each $i \leq N_{total}$ **do**
 - 3: generate the time at which the first collision happens: $t_c = -\frac{\ln \eta}{\frac{\sigma}{\epsilon^2}}$, where $\eta \in (0, 1)$ is a random number from uniform distribution;
 - 4: find the time for free transport $t_f = \min(t_c, \Delta t)$;
 - 5: update particle position $x_i = x_i + \frac{\mu_i}{\epsilon} t_f$;
 - 6: **if** $t_c \leq \Delta t$ **then**
 - 7: find $j = \text{index of cell for } x_i$;
 - 8: add the weight of this particle to macroscopic variable for re-sampling: $W_j = W_j + \frac{w_i}{\Delta x}$;
 - 9: delete information of this particle (x_i, μ_i, w_i) ;
 - 10: **end if**
 - 11: **end for**;
 - 12: Calculate E^{n+1} by solving equation (3.8);
 - 13: Calculate Φ_E by equation (3.11);
 - 14: Evolve W by Φ_E to W^* using $W_j^* = W_j - \frac{\Delta t}{\Delta x} (\Phi_{E, j+\frac{1}{2}} - \Phi_{E, j-\frac{1}{2}})$;
 - 15: Re-sample particles from W^* as described in Section 3.2.2;
 - 16: **return** Distribution of all particles $\cup(x_i, \mu_i, w_i)$ and E^{n+1} .
-

3.3. Properties of the algorithm. The unified gas-kinetic particle method satisfies the following properties:

1. The energy density is conserved.
2. The macroscopic variable E is the summation of contribution from all microscopic particles.
3. In the diffusive limit, $\epsilon \rightarrow 0$ and $e^{-\frac{\sigma_j \Delta t}{\epsilon^2}} \rightarrow 0$, each particle is re-sampled from the equilibrium distribution with probability 1. At the same time, the scheme for updating macroscopic variables tends to the following limiting equation

$$(3.13) \quad \frac{E_j^{n+1} - E_j^n}{\Delta t} - \frac{1}{\Delta x} \left(\frac{1}{3\sigma_{j+\frac{1}{2}}} \frac{E_{j+1}^{n+1} - E_j^{n+1}}{\Delta x} - \frac{1}{3\sigma_{j-\frac{1}{2}}} \frac{E_j^{n+1} - E_{j-1}^{n+1}}{\Delta x} \right) = 0.$$

The algorithm is equivalent to a time-implicit central difference solver of the diffusion equation.

4. In the free transport limit, $\sigma \rightarrow 0$ and $e^{-\frac{\sigma_j \Delta t}{\epsilon^2}} \rightarrow 1$, each particle is traced exactly by free transport with probability 1. In this case, the algorithm could recover the exact

solution for each particle.

3.4. Extension to the coupled equations of gray radiative transfer and material energy. This section extends the unified gas-kinetic particle method to solve the coupled system of gray radiative transfer equation and material temperature equation,

$$(3.14) \quad \begin{cases} \frac{\epsilon^2}{c} \frac{\partial I}{\partial t} + \epsilon\mu \frac{\partial I}{\partial x} = \sigma \left(\frac{1}{2} acT^4 - I \right), \\ \epsilon^2 C_v \frac{\partial T}{\partial t} = \sigma \left(\int_{-1}^1 I(\mu) d\mu - acT^4 \right). \end{cases}$$

Define $u_r = aT^4$ and $\beta = \frac{\partial u_r}{\partial T}$, then the second equation could be re-written as

$$(3.15) \quad \frac{\partial u_r}{\partial t} = C_v^{-1} \beta \frac{\sigma}{\epsilon^2} \left(\int_{-1}^1 I(\mu) d\mu - cu_r \right).$$

The implicit Monte Carlo method proposed by Fleck and Cummings in [10] has been shown to be an effective technique for solving non-linear, time-dependent, radiative transfer problems and is widely used in the radiative transfer community. Fleck's implicit Monte Carlo method uses an effective scattering process to approximate the absorption and emission of radiation by the background medium. This treatment allows it to take larger time steps than that in a purely explicit method. Here the similar semi-implicit discretization for material temperature will be employed. Specifically, Eq. (3.15) is discretized by

$$(3.16) \quad \frac{u_r^{n+1} - u_r^n}{\Delta t} = C_v^{-1} \beta^n \frac{\sigma}{\epsilon^2} (E - cu_r^{n+1}),$$

which gives

$$(3.17) \quad u_r^{n+1} = \frac{1}{1 + cC_v^{-1} \beta^n \times \frac{\sigma \Delta t}{\epsilon^2}} u_r^n + \frac{C_v^{-1} \beta^n \times \frac{\sigma \Delta t}{\epsilon^2}}{1 + cC_v^{-1} \beta^n \times \frac{\sigma \Delta t}{\epsilon^2}} E.$$

With the definition

$$(3.18) \quad \sigma_a = \frac{\sigma}{1 + cC_v^{-1} \beta^n \times \frac{\sigma \Delta t}{\epsilon^2}}, \quad \sigma_s = \sigma - \sigma_a,$$

substituting Eq. (3.17) into Eq. (3.14) yields

$$(3.19) \quad \frac{\epsilon^2}{c} \frac{\partial I}{\partial t} + \epsilon\mu \frac{\partial I}{\partial x} = \sigma_s \left(\frac{1}{2} E - I \right) + \sigma_a \left(\frac{1}{2} cu_r^n - I \right).$$

An operator splitting scheme is used to solve the above system, i.e., for the linear kinetic equation

$$(3.20) \quad \frac{\epsilon^2}{c} \frac{\partial I}{\partial t} + \epsilon\mu \frac{\partial I}{\partial x} = \sigma_s \left(\frac{1}{2} E - I \right),$$

and the radiation energy exchange,

$$(3.21) \quad \frac{\epsilon^2}{c} \frac{\partial I}{\partial t} = \sigma_a \left(\frac{1}{2} cu_r^n - I \right),$$

with the update of material energy through conservation principle. Here Eq. (3.20) is solved using the algorithm introduced in Section 3.2.

The numerical procedure for the updates of radiation-material coupling system is the following. The spatial domain is covered by the mesh points. The variables are the cell averaged E and u_r , as well as the particle positions, velocities, and weights. The discretized absorption coefficient is defined in each cell. First, particle distribution and E are advanced to the next time step by solving Eq. (3.20) using Algorithm 3.1. After the determination of the particle distribution by solving Eq. (3.21), the energy change of particles is added to update u_r through the energy conservation. The process is repeated for the new time step until the end of computation.

4. Numerical Experiments. In this section, we present numerical examples to validate the proposed UGKP method. As we are targeting to develop a method that automatically bridges the optically thin and optically thick regimes, the test cases cover the rarefied ($\epsilon \gg \Delta x$), the intermediate ($\epsilon \approx \Delta x$), and the diffusive ($\epsilon \ll \Delta x$) regimes, as defined in [16]. Depending on the regimes, the numerical results are compared with the solutions of discrete ordinate method and those of the diffusion equation. A large number of grid points are used to ensure the convergence of the reference solutions. All numerical tests are conducted in the one-dimensional slab geometry.

For the UGKP method, the time step is determined by $\Delta t = CFL * \epsilon \Delta x / c$, with $CFL = 0.8$. Therefore, when ϵ is small, i.e. in the diffusive regime, the current method can use a much larger cell size and time step than the particle mean free path and collision time.

4.1. Linear transport equation. Examples in this section are for the linear equation with a possible source term

$$(4.1) \quad \epsilon \frac{\partial I}{\partial t} + \mu \frac{\partial I}{\partial x} = \frac{\sigma}{\epsilon} \left(\frac{1}{2} E - I \right) + \epsilon G.$$

In the following, the results of the unified gas kinetic particle method are obtained using 200 grids in space, and 400 simulation particles within each cell. The final results are from the averages of 10 runs.

EXAMPLE 4.1 (Diffusive regime). Take $\epsilon = 10^{-4}$ and $G = 0$. In this example, we consider a semi-infinite spatial domain $x \in [0, \infty)$ with an isotropic inflow condition imposed on the left boundary. The numerical simulation is in a spatial domain $[0, 1]$. The initial value is $I(\mu) = 0$ for all x . Inflow boundary condition is imposed at $x = 0$ with the incoming specific intensity $I(t, 0, \mu) = \frac{1}{2}$.

The reference solution is obtained from solving the diffusion equation with implicit discretization in time and central differencing in space using 200 grids. Boundary conditions for both the diffusion equation and the macroscopic equation in the unified gas-kinetic particle method are given by $E_{ghost} = 2E_{bd} - E_0$, where E_{ghost} and E_{bd} are the values of E in the ghost cell and the boundary cell respectively. Results for the numerical solution of E are compared at time $t = 0.15$.

This example tests the UGKP method's ability to recover the diffusive regime. Fig. 4.1 shows the solutions from the current scheme, the second order UGKS, and the diffusion equation. These three solutions agree with each other very well. It shows that the unified gas-kinetic particle method can recover the diffusive solution accurately even with the mesh size being much larger than the photon's mean free path.

It should be emphasized that the size of the time step taken in our computation is of the order 10^{-6} , while the mean collision time is of the order 10^{-8} . Therefore, the time step used in the current scheme is around two orders of magnitude larger than the particle mean collision time. This advantage will become even more obvious for smaller ϵ .

EXAMPLE 4.2 (Rarefied regime). The initial and boundary conditions are taken to be the same as the previous example, and also $G = 0$. For this test case, we take $\epsilon = 1$ and run

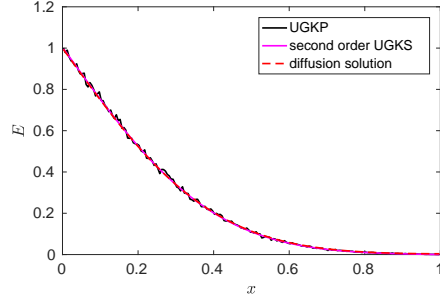


FIG. 4.1. The macroscopic energy densities E as functions of the spatial coordinate x for the diffusive regime at $t = 0.15$.

the computation until $t = 0.9$.

The discrete ordinates method with standard upwind discretization is employed to get the reference solution with 280 points in velocity space and 2000 points in physical space. In Figure 4.2 the results of E are plotted at times $t = 0.1, 0.3, 0.6$ and 0.9 . It is observed that the current solutions have excellent agreement with the reference solutions. This shows the UGKP method could recover accurate solution in the rarefied regime.

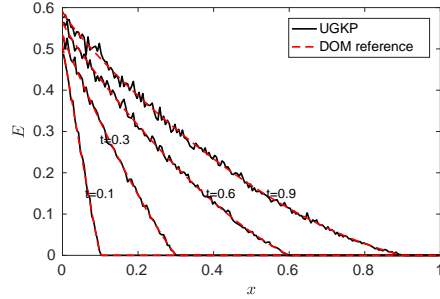


FIG. 4.2. The macroscopic energy densities E as functions of the spatial coordinate x for the rarefied regime at $t = 0.1, 0.3, 0.6$ and 0.9 .

EXAMPLE 4.3 (Intermediate regime with a source term). In this problem, the internal radiation source is given by

$$G = \begin{cases} 1, & \text{if } 0.4 \leq x \leq 0.9, \\ 0, & \text{otherwise.} \end{cases}$$

We take $\epsilon = 10^{-2}$ and $\sigma = 1 + (2x)^5$. The computation domain is $x \in [0, 1]$. The initial value is set as $I = 0$ for all x . The simulation time interval is from $t_0 = 0$ to $t = 0.02$.

The results for E are presented at time $t = 0.02$ in Figure 4.3. The reference solution is obtained from the discrete ordinates method with 2000 points in physical space and 280 points in velocity space. We observe that the result of the UGKP method matches the reference solution very well. It shows that the UGKP is an accurate method in the intermediate regime.

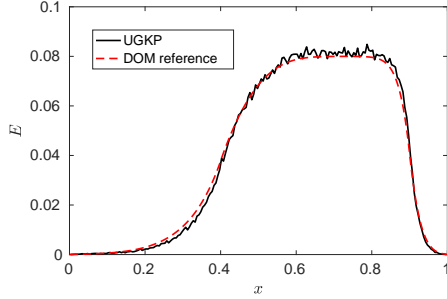


FIG. 4.3. The macroscopic energy densities E as functions of the spatial coordinate x for the intermediate regime at $t = 0.02$.

4.2. Radiation transfer and material energy equations. In order to study the effectiveness of the UGKP method for radiation-material coupling, we simulated Riemann problems for Eq. (3.14) in different regimes. In the following three examples, the parameters σ , c , a and C_V are all set to 1. The computation domain is $x \in [0, 1]$. The initial conditions are

$$(4.2) \quad I(0, x, \mu) = \begin{cases} 1, & \text{if } x \in [0, \frac{1}{2}), \\ \frac{1}{2}, & \text{if } x \in [\frac{1}{2}, 1], \end{cases}$$

and $u_r = E$ for all x . Reflecting boundary conditions are imposed at $x = 0$ and $x = 1$. For all simulations below, the UGKP method always uses 200 grids in space and 4000 simulation particles within each cell. The results are obtained directly without employing multiple computations and averaging.

EXAMPLE 4.4 (Rarefied regime). Take $\epsilon = 1$ and run the computation until $t = 0.3$.

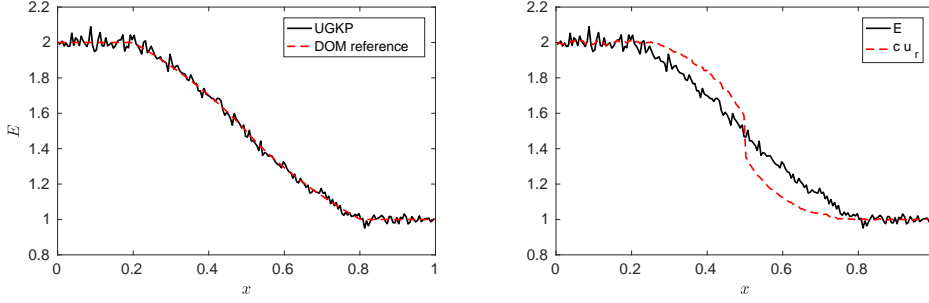
The reference solution is obtained by employing the same splitting technique as outlined in Section 3.4. However, for the reference solution, Eq. (3.20) is solved with the discrete ordinates method under the finite volume framework, using 2000 points in physical space and 280 points in velocity space. As indicated in Fig. 4.4(a), the solution of UGKP method is essentially the same as that of the reference solution. This case validates the accuracy of UGKP method for the problems of radiation-material coupling in the rarefied regime. Fig. 4.4(b) compares the UGKP solution of E and cu_r and they are not in equilibrium in such a rarefied regime.

EXAMPLE 4.5 (Intermediate regime). Take $\epsilon = 10^{-2}$ and run the computation until $t = 0.03$.

The reference solution is obtained in the same way as in the previous example using the same number of discretization points. Fig. 4.5(a) presents the solutions of the UGKP method and the reference one. Both solutions are fairly consistent. The UGKP method is an accurate solver in the intermediate regime. Also, in Fig. 4.5(b) the UGKP solutions of E and cu_r are presented. In this regime, the energy exchange between radiation and the background medium has reached equilibrium at the output time.

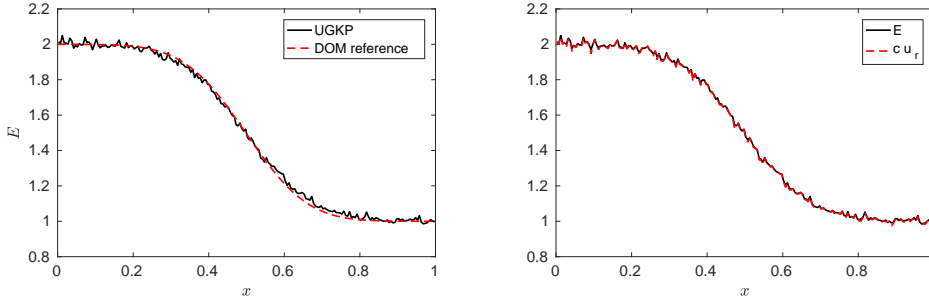
EXAMPLE 4.6 (Diffusive regime). Take $\epsilon = 10^{-4}$ and run the computation until $t = 0.03$.

The reference solution is obtained by solving an equilibrium diffusion equation with central differencing using 200 grid points in space. It was observed in [6] that the implicit Monte Carlo method proposed by Fleck and Cummings is not an asymptotic preserving method for the equilibrium diffusion limit even though the implicit Monte Carlo method is robust and works well in most cases even for time steps being larger than the mean collision time. The



(a) Comparison of the radiation energy density E between UGKP and the DOM reference solution. (b) Comparison between E and cu_r for the UGKP solution.

FIG. 4.4. Numerical results of radiation-material coupling for the rarefied regime at $t = 0.3$.

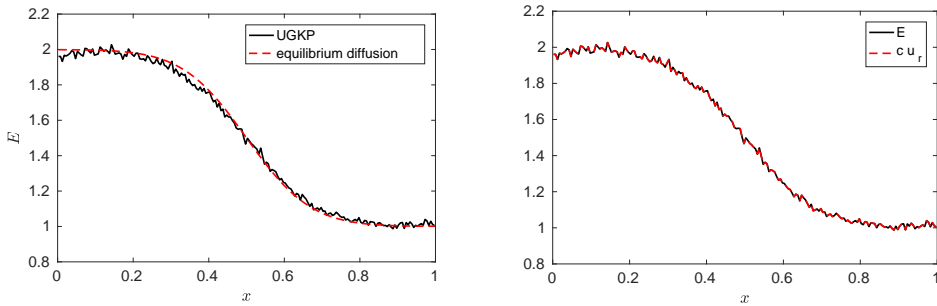


(a) Comparison of the radiation energy density E between UGKP and the DOM reference solution. (b) Comparison between E and cu_r for the UGKP solution.

FIG. 4.5. Numerical results for radiation-material coupling for the intermediate regime at $t = 0.03$.

UGKP solution is given in Fig. 4.6(a), which is the same as the result from the diffusion equation in this diffusive regime. Fig. 4.6(b) displays the solutions for radiation and material energy of UGKP method at $t = 0.03$, which get to equilibrium. This case tests the accuracy of the UGKP method for the coupled radiation-material system in the diffusive regime.

5. Conclusion. In this paper, for the first time a unified gas-kinetic particle method is proposed to simulate radiative transfer. The UGKP method is a multiscale method for the photon transport in different regimes. For the linear transport equation, this method recovers the solution of the diffusion equation in the optically thick limit without constraint on the time step being less than the photon's mean collision time. At the same time, it gives the exact solution in the free transport regime. The UGKP method is also extended to the coupled radiation-material system. With the inclusion of energy exchange, the UGKP method can give excellent simulation results in different regimes. A few benchmark problems are tested to show the performance of the current scheme. The accuracy and efficiency of the UGKP method are fully confirmed. In the future work, we will extend this method to multidimensional and frequency-dependent radiative transfer problems.



(a) Comparison of the radiation energy density E between UGKP and equilibrium diffusion solution. (b) Comparison between E and cu_r for the UGKP solution.

FIG. 4.6. Numerical results for radiation-material coupling for the diffusive regime at $t = 0.03$.

REFERENCES

- [1] G. W. ALLDREDGE, R. LI, AND W. LI, *Approximating the M_2 method by the extended quadrature method of moments for radiative transfer in slab geometry.*, *Kinetic & Related Models*, 9 (2016), pp. 237–249.
- [2] J. A. CARRILLO, T. GOUDON, P. LAFITTE, AND F. VECIL, *Numerical schemes of diffusion asymptotics and moment closures for kinetic equations*, *Journal of Scientific Computing*, 36 (2008), pp. 113–149.
- [3] S.-S. CHEN, B.-W. LI, AND Y.-S. SUN, *Chebyshev collocation spectral method for solving radiative transfer with the modified discrete ordinates formulations*, *International Journal of Heat and Mass Transfer*, 88 (2015), pp. 388–397.
- [4] P. J. COELHO, *Advances in the discrete ordinates and finite volume methods for the solution of radiative heat transfer problems in participating media*, *Journal of Quantitative Spectroscopy and Radiative Transfer*, 145 (2014), pp. 121–146.
- [5] S. W. DAVIS, J. M. STONE, AND Y.-F. JIANG, *A radiation transfer solver for athena using short characteristics*, *The Astrophysical Journal Supplement Series*, 199 (2012), p. 9.
- [6] J. D. DENSMORE AND E. W. LARSEN, *Asymptotic equilibrium diffusion analysis of time-dependent Monte Carlo methods for grey radiative transfer*, *Journal of Computational Physics*, 199 (2004), pp. 175–204.
- [7] J. D. DENSMORE, K. G. THOMPSON, AND T. J. URBATSCH, *A hybrid transport-diffusion Monte Carlo method for frequency-dependent radiative-transfer simulations*, *Journal of Computational Physics*, 231 (2012), pp. 6924–6934.
- [8] J. D. DENSMORE, T. J. URBATSCH, T. M. EVANS, AND M. W. BUKSAS, *A hybrid transport-diffusion method for Monte Carlo radiative-transfer simulations*, *Journal of Computational Physics*, 222 (2007), pp. 485–503.
- [9] J. FLECK AND E. CANFIELD, *A random walk procedure for improving the computational efficiency of the implicit Monte Carlo method for nonlinear radiation transport*, *Journal of Computational Physics*, 54 (1984), pp. 508–523.
- [10] J. FLECK AND J. CUMMINGS, *An implicit Monte Carlo scheme for calculating time and frequency dependent nonlinear radiation transport*, *J. Comput. Phys.*, 8 (1971), pp. 313–342.
- [11] M. FRANK, B. DUBROCA, AND A. KLAR, *Partial moment entropy approximation to radiative heat transfer*, *Journal of Computational Physics*, 218 (2006), pp. 1–18.
- [12] J. GIORLA AND R. SENTIS, *A random walk method for solving radiative transfer equations*, *Journal of Computational Physics*, 70 (1987), pp. 145–165.
- [13] C. K. HAYAKAWA, J. SPANIER, AND V. VENUGOPALAN, *Coupled forward-adjoint Monte Carlo simulations of radiative transport for the study of optical probe design in heterogeneous tissues*, *SIAM Journal on Applied Mathematics*, 68 (2007), pp. 253–270.
- [14] B. HUNTER AND Z. GUO, *Comparison of quadrature schemes in DOM for anisotropic scattering radiative transfer analysis*, *Numerical Heat Transfer, Part B: Fundamentals*, 63 (2013), pp. 485–507.
- [15] S. JIN, *Efficient asymptotic-preserving (AP) schemes for some multiscale kinetic equations*, *SIAM Journal on Scientific Computing*, 21 (1999), pp. 441–454.
- [16] S. JIN, L. PARESCHI, AND G. TOSCANI, *Diffusive relaxation schemes for multiscale discrete-velocity kinetic equations*, *SIAM Journal on Numerical Analysis*, 35 (1998), pp. 2405–2439.
- [17] S. JIN, L. PARESCHI, AND G. TOSCANI, *Uniformly accurate diffusive relaxation schemes for multiscale*

- transport equations*, SIAM Journal on Numerical Analysis, 38 (2000), pp. 913–936.
- [18] A. KLAR, *An asymptotic-induced scheme for nonstationary transport equations in the diffusive limit*, SIAM journal on numerical analysis, 35 (1998), pp. 1073–1094.
- [19] A. D. KLOSE, U. NETZ, J. BEUTHAN, AND A. H. HIELSCHER, *Optical tomography using the time-independent equation of radiative transfer-Part 1: forward model*, Journal of Quantitative Spectroscopy and Radiative Transfer, 72 (2002), pp. 691–713.
- [20] C. LIU, Z. WANG, AND K. XU, *A unified gas-kinetic scheme for continuum and rarefied flows VI: dilute disperse gas-particle multiphase system*, arXiv preprint arXiv:1802.04961, (2018).
- [21] C. LIU AND K. XU, *A unified gas kinetic scheme for continuum and rarefied flows V: multiscale and multi-component plasma transport*, Communications in Computational Physics, 22 (2017), pp. 1175–1223.
- [22] L. LUCY, *Computing radiative equilibria with Monte Carlo techniques*, Astronomy and Astrophysics, 344 (1999), pp. 282–288.
- [23] A. MARSHAK AND A. DAVIS, *3D radiative transfer in cloudy atmospheres*, Springer Science & Business Media, 2005.
- [24] L. MIEUSSENS, *On the asymptotic preserving property of the unified gas kinetic scheme for the diffusion limit of linear kinetic models*, Journal of Computational Physics, 253 (2013), pp. 138–156.
- [25] G. NALDI AND L. PARESCHI, *Numerical schemes for kinetic equations in diffusive regimes*, Applied mathematics letters, 11 (1998), pp. 29–35.
- [26] T. ROOS, T. HARMS, AND C. DU TOIT, *Conservation of scattered energy and asymmetry factor in the new rotationally symmetric spherical discretisation scheme*, International Journal of Heat and Mass Transfer, 101 (2016), pp. 205–225.
- [27] W. SUN, S. JIANG, AND K. XU, *An asymptotic preserving unified gas kinetic scheme for gray radiative transfer equations*, Journal of Computational Physics, 285 (2015), pp. 265–279.
- [28] W. SUN, S. JIANG, AND K. XU, *An implicit unified gas kinetic scheme for radiative transfer with equilibrium and non-equilibrium diffusive limits*, Communications in Computational Physics, 22 (2017), pp. 889–912.
- [29] W. SUN, S. JIANG, AND K. XU, *A multidimensional unified gas-kinetic scheme for radiative transfer equations on unstructured mesh*, Journal of Computational Physics, 351 (2017), pp. 455–472.
- [30] W. SUN, S. JIANG, AND K. XU, *An asymptotic preserving implicit unified gas kinetic scheme for frequency-dependent radiative transfer equations*, International Journal of Numerical Analysis & Modeling, 15 (2018), pp. 134–153.
- [31] W. SUN, S. JIANG, K. XU, AND S. LI, *An asymptotic preserving unified gas kinetic scheme for frequency-dependent radiative transfer equations*, Journal of Computational Physics, 302 (2015), pp. 222–238.
- [32] V. VIKAS, C. HAUCK, Z. WANG, AND R. O. FOX, *Radiation transport modeling using extended quadrature method of moments*, Journal of Computational Physics, 246 (2013), pp. 221–241.
- [33] K. XU, *Direct modeling for computational fluid dynamics: construction and application of unified gas-kinetic schemes*, World Scientific, 2015.
- [34] K. XU AND J.-C. HUANG, *A unified gas-kinetic scheme for continuum and rarefied flows*, Journal of Computational Physics, 229 (2010), pp. 7747–7764.